Earthq Eng & Eng Vib (2014) 13: 671-680 **DOI**:10.1007/s11803-014-0271-8

Experimental validation of a signal-based approach for structural earthquake damage detection using fractal dimension of time frequency feature

Tao Dongwang[1†], Mao Chenxi[1‡], Zhang Dongyu[2,3†] and Li Hui[2,3‡]

1. *Key Laboratory of Earthquake Engineering and Engineering Vibration*, *Institute of Engineering Mechanics, China Earthquake Administration, Harbin 150080, China*
2. *Key Lab of Structures Dynamic Behavior and Control* (*Harbin Institute of Technology*)*, Ministry of Education, Harbin 150090, China*
3. *Center of Structural Monitoring and Control, School of Civil Engineeing, Harbin Institute of Technology, Harbin 150090, China*

Abstract: This article extends a signal-based approach formerly proposed by the authors, which utilizes the fractal dimension of time frequency feature (FDTFF) of displacements, for earthquake damage detection of moment resist frame (MRF), and validates the approach with shaking table tests. The time frequency feature (TFF) of the relative displacement at measured story is defined as the real part of the coefficients of the analytical wavelet transform. The fractal dimension (FD) is to quantify the TFF within the fundamental frequency band using box counting method. It is verified that the FDTFFs at all stories of the linear MRF are identical with the help of static condensation method and modal superposition principle, while the FDTFFs at the stories with localized nonlinearities due to damage will be different from those at the stories without nonlinearities using the reverse-path methodology. By comparing the FDTFFs of displacements at measured stories in a structure, the damage-induced nonlinearity of the structure under strong ground motion can be detected and localized. Finally shaking table experiments on a 1:8 scale sixteen-story three-bay steel MRF with added frictional dampers, which generate local nonlinearities, are conducted to validate the approach.

Keywords: earthquake damage detection; time frequency feature; fractal dimension; signal-based; shaking table test; frictional damper

1 Introduction

Strong earthquakes have caused great damage to civil structures in the past few years. It is in great demand that structural safety assessment should be provided immediately after an earthquake in order to implement post-event emergency, rescue and reconstruction. The recently developed structural health monitoring (SHM) systems have been widely implemented in civil structures to monitor the real-time responses under actual ambient excitations, winds and earthquakes (Ou and Li, 2010; Kalkan *et al*., 2012). They can detect damage at an early age and issue a warning during a hazard, and also provide reliable information on the safety of the structure after extreme events such as earthquakes or strong winds. In the past two decades, vibration-based damage detection methods have been developed for SHM, however most of them assume the structure is linear before and after damage (Doebling *et al*., 1996; Sohn *et al*., 2004; Farrar *et al*., 2007). It is well known that the civil structures will exhibit inelastic and nonlinear behavior due to the material and geometrical nonlinearities under strong ground motion, and this is the distinctiveness of earthquake damage of structures, which can be used for damage detection. Recently there is a trend using nonlinear features or nonlinear system identification methods for earthquake damage detection (Farrar *et al*., 2007; Chanpheng *et al*., 2012). These methods are mainly classified into signal-based and model-based groups. Model-based methods assume a mathematical description for the nonlinear force-displacement relation such as the Bouc-Wen model, and identify the parameters of the model using the measured excitation and responses (Wu and Smyth, 2007). The advantage of model-based approaches is that they can

Correspondence to: Li Hui, School of Civil Engineering, Harbin Institute of Technology, Harbin 150090, China
Tel: +86-451-86282013
E-mail: lihui@hit.edu.cn
†Assisstant Researcher; ‡Professor

Supported by: National Natural Science Foundation under Grant No. 51161120359, Ministry of Education under Grant No. 20112302110050 and Special Fund for Earthquake Scientific Research in the Public Interest under Grant No. 201308003

Received June 24, 2013; **Accepted** January 15, 2014

quantify the extent of damage using certain damage index such as that proposed by Park and Ang with the help of estimated hysteretic curves (Park *et al*., 1985). However, the real behavior of a large civil structure under strong ground motion is too complicated to be described by a nonlinear model even the modified Bouc-Wen model. Meanwhile the model-based methods typically assume the masses of the structure are known beforehand, which may be not available for real problems. On the other hand, the signal-based methods just detect the nonlinear features obtained from measured responses or the corresponding spectra using signal processing methods (Loh *et al*., 2010; Chanpheng *et al*., 2012). Depending on the domain of signal processing, the signal-based methods are divided into time domain, frequency domain and time-frequency domain methods (Qiao and Esmaeily, 2011). Because the ground motion and the structural responses are nonstationary in nature as the amplitude and frequency contents evolve with time, the time-frequency methods receive much attention in earthquake damage detection due to their ability to analyze nonstationary signals (Spanos *et al*., 2007). The corresponding nonlinear feature can be the coefficients of discrete or continuous wavelet transform and their derived quantities such as the mean or instantaneous frequency, energy in specific frequency or time range (Loh *et al*., 2010). The detail coefficients of discrete wavelet transform were used to detect the time instant when the structural stiffness changed due to damage (Hou *et al*., 2000). The coefficients of continuous wavelet transform were used to identify the frequency variation between yielding and unloading of a bilinear structure under ground motion (Pan and Lee, 2002). Mean instantaneous frequency of relative acceleration was proposed to detect and track earthquake damage using adaptive wavelet decomposition and empirical mode decomposition (Spanos *et al*., 2007). The first instantaneous system frequency determined from the ridge of Gabor transform of relative displacement was treated as an indicator of the existence of damage (Todorovska and Trifunac, 2007). Several signal-based method using time-frequency analysis such as Hilbert marginal spectrum, the instantaneous mean frequency, the Holder exponent and wavelet component energy distribution are applied to detect earthquake damage (Loh *et al*., 2010). Single and multiple earthquake damages of shear-type building were identified by comparing the fractal dimensions of time-frequency features at different degree of freedoms (Li *et al*., 2013). A general review on time-frequency domain damage detection methods such as short-time Fourier transform, empirical mode decomposition and wavelet transform was given (Nagarajaiah and Basu, 2009).

The objective of this article is to utilize the approach by Li *et al*. (2013) and extend it from shear-type building to MRF and validate it by conducting shaking table tests. Structural earthquake damages are caused by the yielding of structural components, and the structure has local damage-induced nonlinearities. Due to the local nonlinearities, the story with damage cannot keep the same mode shape oscillation and phases with others, and the corresponding irregularity or complexity of the TFF is different from others (Li *et al*., 2013). The FDTFF at story with nonlinearity may be larger or smaller than those without nonlinearities. Therefore FDTFF can be referred as a localization indicator of damage-induced nonlinearity. By comparing the indicators at different stories, the damaged story due to material nonlinearity can be detected and localized. This signal-based approach only requires the measurements of the damaged structure and does not need the corresponding structural model. Meanwhile, shaking table test on a 1:8 scale sixteen-story three-bay steel MRF is used to validate the signal-based approach for damage-induced nonlinearity detection, where frictional dampers are installed at some stories to model single or multiple local nonlinearities.

2 Methodology of earthquake damage detection of MRF using FDTFF

For MRF, usually only the translational degree of freedoms (DOF) are measured, and the motion equation of linear MRF, ignoring the inertial effect of beams, is given by

$$\begin{bmatrix} \boldsymbol{M}_{\mathrm{mm}} & \boldsymbol{0} \\ \boldsymbol{0} & \boldsymbol{0} \end{bmatrix} \begin{Bmatrix} \ddot{\boldsymbol{X}}_{\mathrm{m}} \\ \ddot{\boldsymbol{X}}_{\mathrm{s}} \end{Bmatrix} + \begin{bmatrix} \alpha \boldsymbol{M}_{\mathrm{mm}} + \beta \boldsymbol{K}_{\mathrm{mm}} & \beta \boldsymbol{K}_{\mathrm{ms}} \\ \beta \boldsymbol{K}_{\mathrm{sm}} & \beta \boldsymbol{K}_{\mathrm{ss}} \end{bmatrix} \begin{Bmatrix} \dot{\boldsymbol{X}}_{\mathrm{m}} \\ \dot{\boldsymbol{X}}_{\mathrm{s}} \end{Bmatrix} + \begin{bmatrix} \boldsymbol{K}_{\mathrm{mm}} & \boldsymbol{K}_{\mathrm{ms}} \\ \boldsymbol{K}_{\mathrm{sm}} & \boldsymbol{K}_{\mathrm{ss}} \end{bmatrix} \cdot \begin{Bmatrix} \boldsymbol{X}_{\mathrm{m}} \\ \boldsymbol{X}_{\mathrm{s}} \end{Bmatrix} = -\begin{bmatrix} \boldsymbol{M}_{\mathrm{mm}} & \boldsymbol{0} \\ \boldsymbol{0} & \boldsymbol{0} \end{bmatrix} \ddot{x}_{\mathrm{g}}(t) \tag{1}$$

where subscripts "m" and "s" denote the main or translational DOF and the secondary or rotational DOF of the frame with displacement vectors $\boldsymbol{X}_{\mathrm{m}} = [x_1, x_2, \cdots x_{N_{\mathrm{s}}}]^{\mathrm{T}}$, $\boldsymbol{X}_{\mathrm{s}} = [\theta_1, \theta_2, \cdots, \theta_{N_{\mathrm{s}} \times (N_{\mathrm{b}}+1)}]^{\mathrm{T}}$, where N_{s} is the number of stores, N_{b} is the number of bays of the frame and superscript T is the transpose operator; $\dot{\boldsymbol{X}}_{\mathrm{m}}$, $\ddot{\boldsymbol{X}}_{\mathrm{m}}$ are the corresponding translational velocity and acceleration vectors; $\boldsymbol{M}_{\mathrm{mm}}$, $\boldsymbol{C}_{\mathrm{mm}}$, $\boldsymbol{K}_{\mathrm{mm}}$ are the translational block matrices of mass, stiffness and damping matrices of the structure, and similar for other block matrices; $\ddot{x}_{\mathrm{g}}$ is the ground motion; α and β are the parameters for Rayleigh proportional damping. Based on Eq. (1), it can be deduced that

$$\boldsymbol{X}_{\mathrm{s}} = -\boldsymbol{K}_{\mathrm{ss}}^{-1} \boldsymbol{K}_{\mathrm{sm}} \boldsymbol{X}_{\mathrm{m}} \tag{2}$$

$$\boldsymbol{M}_{\mathrm{mm}} \ddot{\boldsymbol{X}}_{\mathrm{m}} + (\alpha \boldsymbol{M}_{\mathrm{mm}} + \beta(\boldsymbol{K}_{\mathrm{mm}} - \boldsymbol{K}_{\mathrm{ms}} \boldsymbol{K}_{\mathrm{ss}}^{-1} \boldsymbol{K}_{\mathrm{sm}})) \dot{\boldsymbol{X}}_{\mathrm{m}} + (\boldsymbol{K}_{\mathrm{mm}} - \boldsymbol{K}_{\mathrm{ms}} \boldsymbol{K}_{\mathrm{ss}}^{-1} \boldsymbol{K}_{\mathrm{sm}}) \boldsymbol{X}_{\mathrm{m}} = -\boldsymbol{M}_{\mathrm{mm}} \ddot{x}_{\mathrm{g}}(t) \tag{3}$$

Equation (3) can be written as

$$\boldsymbol{M}^{\mathrm{e}}\ddot{\boldsymbol{X}}_{\mathrm{m}}(t)+\boldsymbol{C}^{\mathrm{e}}\dot{\boldsymbol{X}}_{\mathrm{m}}(t)+\boldsymbol{K}^{\mathrm{e}}\boldsymbol{X}_{\mathrm{m}}(t)=-\boldsymbol{M}^{\mathrm{e}}\boldsymbol{1}\ddot{x}_{\mathrm{g}}(t) \quad (4)$$

where $\boldsymbol{M}^{\mathrm{e}}=\boldsymbol{M}_{\mathrm{mm}}$, $\boldsymbol{K}^{\mathrm{e}}=\boldsymbol{K}_{\mathrm{mm}}-\boldsymbol{K}_{\mathrm{ms}}\boldsymbol{K}_{\mathrm{ss}}^{-1}\boldsymbol{K}_{\mathrm{sm}}$ and $\boldsymbol{C}^{\mathrm{e}}=\alpha\boldsymbol{M}^{\mathrm{e}}+\beta\boldsymbol{K}^{\mathrm{e}}$ are the effective mass, stiffness and damping matrices for the condensed MRF.

Using the modal decomposition method, the relative translational displacements of the condensed MRF is obtained

$$\boldsymbol{X}_{\mathrm{m}}(t)=\sum_{i=1}^{n}\boldsymbol{\varphi}_i q_i(t) \quad (5)$$

where $\boldsymbol{\varphi}_i=\left[\varphi_{1i}\ \ \varphi_{2i}\ \ \cdots\ \ \varphi_{Nsi}\right]^{\mathrm{T}}$ is the ith mode-shape vector, q_i is the ith generalized modal coordinator and n is the number of modes involved in the oscillation. The Gabor wavelet transform for each $x_{\mathrm{m}i}$ in $\boldsymbol{X}_{\mathrm{m}}$ is

$$\begin{aligned}Wx_{\mathrm{m}i}(b,a)&=\int_{-\infty}^{\infty}x_{\mathrm{m}i}(t)\frac{1}{\sqrt{a}}\psi^{*}\left(\frac{t-b}{a}\right)\mathrm{d}t=\\&\int_{-\infty}^{\infty}\sum_{j=1}^{n}\phi_{ij}q_j(t)\frac{1}{\sqrt{a}}\psi^{*}\left(\frac{t-b}{a}\right)\mathrm{d}t=\sum_{j=1}^{n}\phi_{ij}Wq_j(b,a)\end{aligned} \quad (6)$$

Taking the real part of both sides of Eq. (6) and using the definition of TFF, which is the real part of the coefficients of the Gabor wavelet transform, it can be obtained

$$F_{x_{\mathrm{m}i}}=W^{\mathrm{r}}x_{\mathrm{m}i}(b,a)=\sum_{j=1}^{n}\phi_{ij}W^{\mathrm{r}}q_j(b,a)=\sum_{j=1}^{n}\Delta\phi_{ij}F_{q_j} \quad (7)$$

The detail of TFF and the calculation of FD can be found in the former paper by the authors (Li *et al*., 2013). The TFF of the ith relative displacement contributed by the jth mode is give by

$$F_{x_{\mathrm{m}i,j}}=W^{\mathrm{r}}x_{\mathrm{m}i,j}(b,a)=\phi_{ij}W^{\mathrm{r}}q_j(b,a)=\phi_{ij}F_{q_j} \quad (8)$$

Based on the property of FD that the FD of a fractal times any constant is equal to the FD of the original fractal, the following equation can be deduced

$$\dim_{\mathrm{B}}(F_{\Delta x_{\mathrm{m}i,j}})=\dim_{\mathrm{B}}(\phi_{ij}F_{q_j})=\dim_{\mathrm{B}}(F_{q_j}) \quad (9)$$

From Eq. (9), it can be seen that the FDs of the TFF of all relative translational displacements of a MRF contributed by a given mode are identical to the FD of that generalized model coordinator. Because the structural response under ground motion is mainly dominated by the first mode, the TFF contributed by the first mode is used for further damage detection given by

$$F_{x_{\mathrm{m},i}}^{\mathrm{d}}=F_{x_{\mathrm{m},i}}(t,f\mid f\in[f_{\mathrm{1l}}\ f_{\mathrm{1h}}]) \quad (10)$$

where f_{1l} and f_{1h} are the corresponding low and high cutoff frequency of the first mode, which is determined form the Fourier Amplitude Spectrum of the measured response such that the chosen frequency band is least affected by other modes. Thus the FDTFF for the ith translational relative displacement is defined as

$$D_i=\dim_{\mathrm{B}}(F_{x_{\mathrm{m},i}}^{\mathrm{d}}) \quad (11)$$

According to the reverse-path methodology (Rice and Fitzpatrick, 1991) for nonlinear parameter estimation, for a MRF having local damage-induced nonlinearity, the motion equation can be written as, treating the state-dependent nonlinear restoring force as external force

$$\begin{aligned}&\boldsymbol{M}^{(\mathrm{l})}\ddot{\boldsymbol{X}}(t)+\boldsymbol{C}^{(\mathrm{l})}\dot{\boldsymbol{X}}(t)+\boldsymbol{K}^{(\mathrm{l})}\boldsymbol{X}(t)=\\&-\boldsymbol{M}^{(\mathrm{l})}\boldsymbol{1}\ddot{x}_{\mathrm{g}}(t)-R(\boldsymbol{X}(t),\dot{\boldsymbol{X}}(t))\end{aligned} \quad (12)$$

where $\boldsymbol{M}^{(\mathrm{l})}$, $\boldsymbol{C}^{(\mathrm{l})}$ and $\boldsymbol{K}^{(\mathrm{l})}$ are the underlying linear mass, damping and stiffness matrices corresponding to the master DOFs respectively. For simplicity the subscripts "m" of the translational relative displacements are omitted. $R(t)$ is the nonlinear restoring force due to local damage. It is noted that the underlying linear damping and stiffness matrices may be different from those when there is no damage, because the local damage may introduce additive damping ratio and stiffness. Suppose the damage is located at the pth story, the pth element r_p of $R(t)$ can be described as a complicated function such as Chebyshev polynomials of the pth inter-story drift and velocity thereof (Masri *et al*., 1982)

$$r_p(t)=T(\Delta x_p)T(\Delta\dot{x}_p) \quad (13)$$

where T is the Chebyshev polynomial and $\Delta x_p=x_p-x_{p-1}$ is the inter-story drift at the pth story. In this way the nonlinear restoring force can be written with its elements as

$$R(t)=\left[\overbrace{0\ \ \cdots\ \ 0}^{p-2}\ \ r_p\ \ -r_p\ \ \overbrace{0\ \ \cdots\ \ 0}^{N_{\mathrm{s}}-p}\right]^{\mathrm{T}} \quad (14)$$

Thus the Eq. (12) can be written in the frequency domain as

$$-\begin{bmatrix} H_{1\ddot{x}_g}(\omega) \\ H_{2\ddot{x}_g}(\omega) \\ \vdots \\ H_{(p-1)\ddot{x}_g}(\omega) \\ H_{p\ddot{x}_g}(\omega) \\ \vdots \\ H_{N_s\ddot{x}_g}(\omega) \end{bmatrix} X_g(\omega) - \begin{bmatrix} H_{1p}(\omega) - H_{1(p-1)}(\omega) \\ H_{2p}(\omega) - H_{2(p-1)}(\omega) \\ \vdots \\ H_{(p-1)p}(\omega) - H_{(p-1)(p-1)}(\omega) \\ H_{pp}(\omega) - H_{p(p-1)}(\omega) \\ \vdots \\ H_{N_s p}(\omega) - H_{N_s(p-1)}(\omega) \end{bmatrix} R_p(\omega) = \begin{bmatrix} X_1(\omega) \\ X_2(\omega) \\ \vdots \\ X_{(p-1)}(\omega) \\ X_p(\omega) \\ \vdots \\ X_{N_s}(\omega) \end{bmatrix} \tag{15}$$

where $H_{i\ddot{x}_g}(\omega)$, i = 1, 2, ···N_s, is the transfer function from the ground motion to the relative displacement at ith story of the underlying linear system; $X_g(\omega)$ and $X_i(\omega)$ are the Fourier transforms of the ground motion and the relative displacement at the ith story respectively; $H_{ip}(\omega)$ is the transfer function from the force excited at pth story to the relative displacement at the ith story, which represents the local nonlinearity effect on the response of other stories; It is similar for $H_{i(p-1)}(\omega)$; $R_p(\omega)$ is the Fourier transform of the nonlinear restoring force generated at pth story. From Eq. (15), it can be deduced that if a story i is far from the pth story, then $H_{ip}(\omega) - H_{i(p-1)}(\omega)$ approximates zero, and the Fourier transform of the relative displacement $X_i(\omega)$ at that story is dominated by $H_{i\ddot{x}_g}(\omega)X_g(\omega)$. Therefore, from Eqs. (9) - (11), the FDTFFs at the stories away from the pth story will almost be the same. As for the stories near the nonlinear story, though $H_{ip}(\omega) - H_{i(p-1)}(\omega)$ cannot be neglected, the FDTFF can be very close to those far away from nonlinear story by carefully choosing the frequency band, i.e. the low and high cutting off frequency for the TFF. As for the pth story, due to the $R_p(\omega)$ is related with x_p, the nonlinearity will cause change in frequency magnitude and phase spectrum, and the FDTFF will be much different from those at other stories since the TFF contains comprehensive frequency amplitude and phase spectra information. Thus by comparing the FDTFF at measured stories, damage-induced nonlinearity in a structure excited by strong ground motion can be detected and localized.

3 Shaking table test validation

3.1 Building model and test facilities

Earthquake shaking table test is carried out to validate the signal-based method. The test structure is a 1:8 scale sixteen-story steel MRF with three bays along the shaking direction and two-pieces in the other direction, as shown in Fig. 1(a). The yielding stress and Young′s modulus of the steel are 215 MPa and 206 GPa, respectively. The height of each story is 0.5 m, and the length of each beam parallel to and perpendicular to the shaking direction are 0.75 m and 1.0 m respectively. The square cross section of column is $50\times50\times4$ (mm) and the wide flange beam section is $60\times4\times30\times5$ (mm). Additional weight added to each floor is 300 kg. To generate local nonlinearities, frictional dampers are installed at some stories, shown in Figs. 1(b) and 1(c). The mechanism of frictional damper is dry friction. It produces resistant force equal to the loading force when the damper is in its stick state when there is no relative motion on the friction interface. When the damper is in its slip state, the frictional damper gives constant resistant force which is proportional to the normal press force, which is dependent on the torque moment applied to the high strength friction grip bolt. The displacement-force relation is strongly nonlinear. Seventeen PCB accelerometers are mounted at the centers of the girders of all floors and the shaking table to measure the corresponding absolute accelerations. Eleven LVDTs are mounted at the centers of girders of floors one to ten and the shaking table to measure the corresponding absolute displacements. The locations of the sensors on the beams are shown in Fig. 1(d). For each frictional damper, a LVDT is mounted to measure the relative slip and a load cell is mounted to measure the damper force.

The accelerations are acquainted using the LMS Test Lab with sampling frequency of 100 Hz, and the displacements and damper force are acquainted using the dSPACE with sampling frequency of 100 Hz. The experimental program is conducted using the uni-axis shaking table in the Structural and Earthquake-resist Testing Center of the School of Civil Engineering at Harbin Institute of Technology, China. The payload is 15 metric tons, and the length of the table along the shaking direction is 4 m and the other is 3 m. The maximum actuator stroke of the shaker is ±125 mm with the maximum horizontal acceleration of ±1.33 g and velocity of ±600 mm/s , and the frequency range is 0–30 Hz. The El Centro (I-ELC180) during the Imperial Valley earthquake of 18 May 1940 (PEER, 2013) is used as the input ground motion for the shaking table tests. The time interval is scaled down by the square root of prototype scale, i.e., from original 0.01 s to 0.035 s. To prevent torsional motion of the tested structure, only ground motion with small PGA is used as excitation. To simulate single and multiple local nonlinearities,

Fig. 1 Photos of the sixteen story 1:8 scale building model: (a) The test frame, damper installed and instruments; (b) The locations of dampers; (c) Close-up of the damper; (d) Close-up of the locations of PCB acceleration and LVDT

four cases with different locations of frictional dampers installed are conducted for the shaking-table test, which are (1) without dampers; (2) with dampers installed at story one; (3) with dampers installed at both story one and story six. The ground motion, damper locations and measured PGA of the shaking table are shown in Table 1.

3.2 Test results

Under the bandwidth white noise excitation with PGA = 18.7 gal, the measured Frequency Response Function and identified FRF for the top story using the relative accelerations are shown in Fig. 2. From the identified system poles, the identified frequencies for the first three modes of the pure frame are 2.14, 6.53 and 8.89 Hz, respectively, and the damping ratios are 1.76%, 0.56% and 0.48%, respectively.

Table 1 The cases of shaking table test

Ground motion	Measured PGA (gal)	Damper locations
El Centro	24.4	None
	26.0	Story One
	43.8	Story One and Six

One time-scaled El Centro ground motion is concatenated to the other to make sure the shaking endures long enough. Figure 3 shows a concatenated time-scaled El Centro ground motion measured at the shaking table. When the pure MRF is subjected to the ground motion, the system behaves in linear range. The time histories (TH), TFFs and Fourier Amplitude Spectra (FAS) of the relative displacements at story one, six and ten, for simplicity, are shown in Fig. 4, where only the

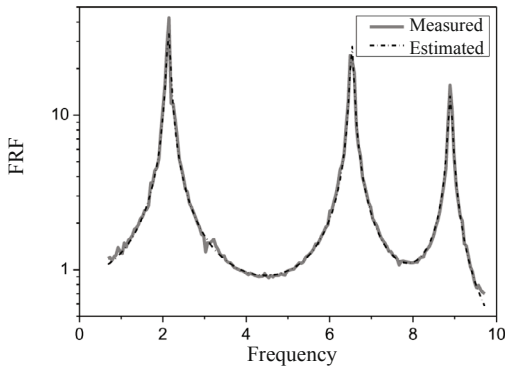

Fig. 2 Measured and estimated frequency response function at the top story

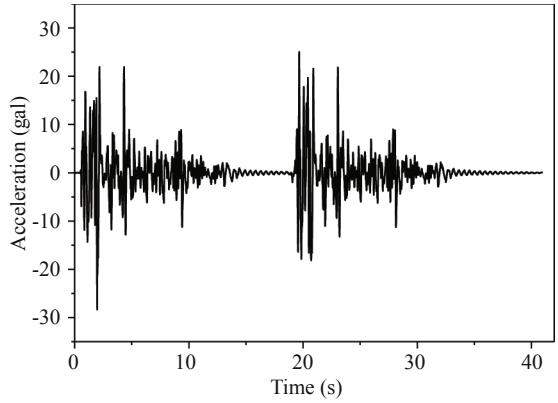

Fig. 3 Concatenated time-scaled El Centro ground motion

TFFs covering the first natural frequency are shown. The TFF is obtained using the Gabor wavelet transform with parameters $f_0 = 2.4$ Hz, $\sigma = 2$, and the low and high cutting off frequency is 1.3 and 3.0 Hz respectively. With the fractal analysis toolbox FRACLAB developed at INRIA (Canus *et al*., 2013), the log-log plots of the chosen TFFs are shown in Fig. 5, from which it can be seen that the TFFs have fractal characteristics in the scale range of 2^{-4}–2^{-2}. The corresponding FDTFF are 2.411, 2.413 and 2.412 for the relative displacements at story one, six and ten, respectively. The TFFs of the relative displacements at other stories have similar fractal characteristics, and the FDTFFs are shown in Fig. 6(a), where it can be seen that the FDTFFs are almost the same.

When frictional dampers are installed at story one of the MRF, the whole system behaves nonlinearly due to the local nonlinearity generated by the frictional dampers, which can be deduced from Eq. (15) where the Fourier transform of the local nonlinear force generated from the frictional dampers will distort the frequency response function of the underlying linear system. From Eq. (15), it can also be seen that the local nonlinear component will cause the whole structure exhibit nonlinearity, and the extent of the nonlinearity depends on the size of the force generated by the local nonlinear component. To check the extent of nonlinearity, it is necessary to compare the damper force to the total restoring force at the same story. The force-displacements for the frictional dampers A and B on two pieces are shown in Fig. 7. The two data acquisitions (DAQ) systems are synchronized by setting the relative displacements at the tenth story have the largest correlation coefficient. The relative displacement in LMS Test Lab is obtained by double integrating the relative acceleration and filtered by a 8th order Butterworth bandpass filter. The bandpass frequency is [0.6 10] Hz. The relative displacements from the two DAQ systems are shown in Fig. 8, which shows good synchronization results. The resistant force generated by the dampers and the total restoring force at story one are shown in Fig. 9. From Fig. 9, it can be seen that the damper force is comparable to the total initial force, which means the local nonlinearity generated by the frictional damper is not negligible.

The THs, TFFs and FAS of the relative displacements

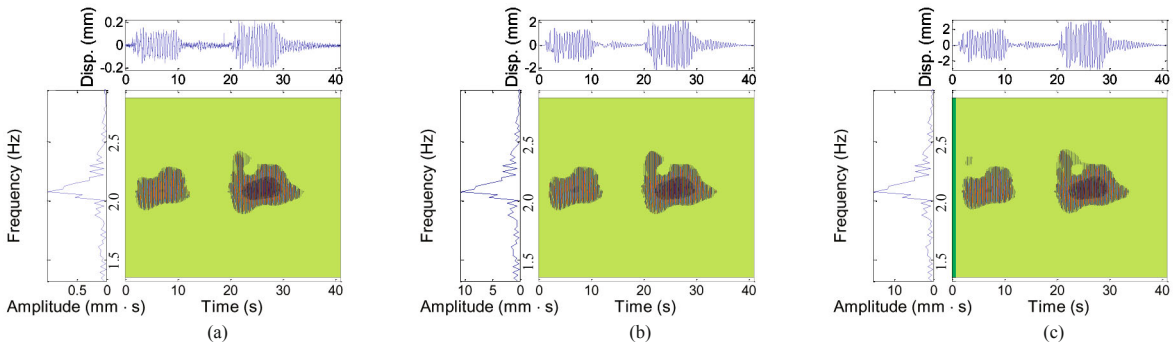

Fig. 4 The THs, TFFs and FAS of relative displacements of the pure MRF under El Centro ground motion: (a) story one, (b) story six; and (c) story ten

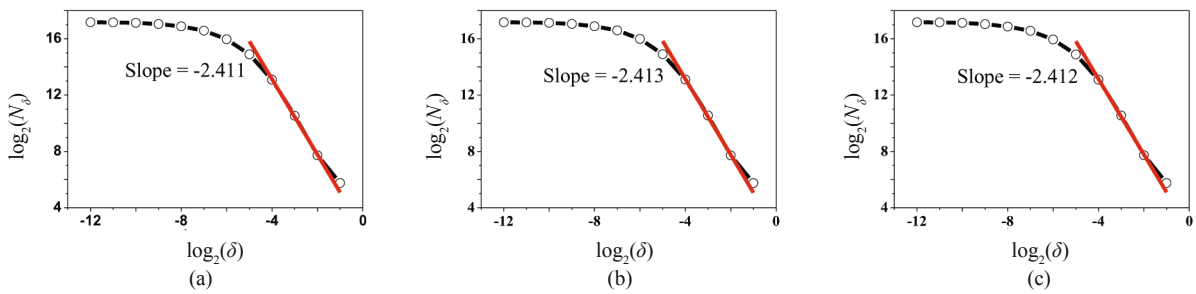

Fig. 5 Log-log plot of the box counting of the TFF of relative displacements of the pure MRF under El Centro ground motion: (a) story one; (b) story six; and (c) story ten

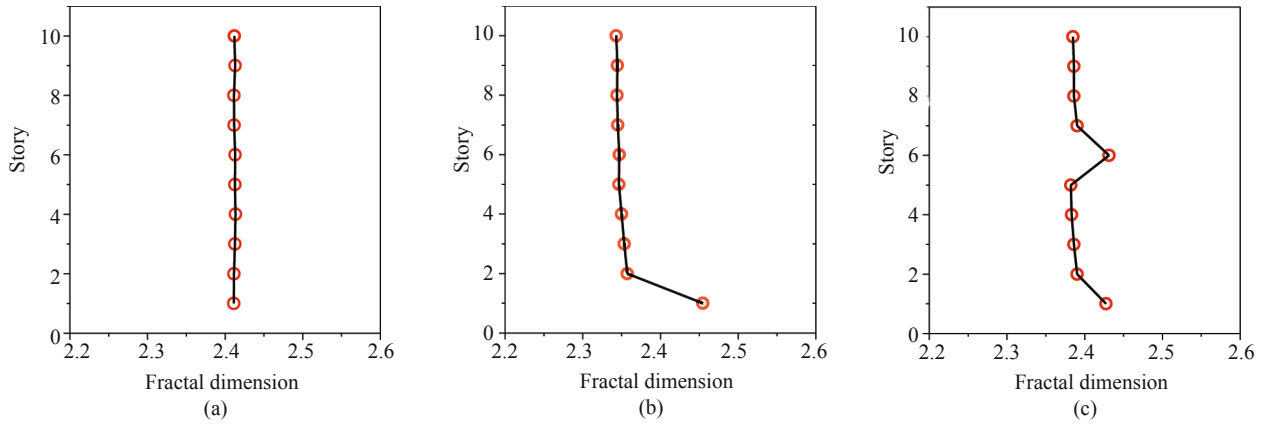

Fig. 6 The FDTFFs of relative displacements of the MRF w/o frictional dampers under El Centro ground motion: (a) none; (b) story one; and (c) story one and six

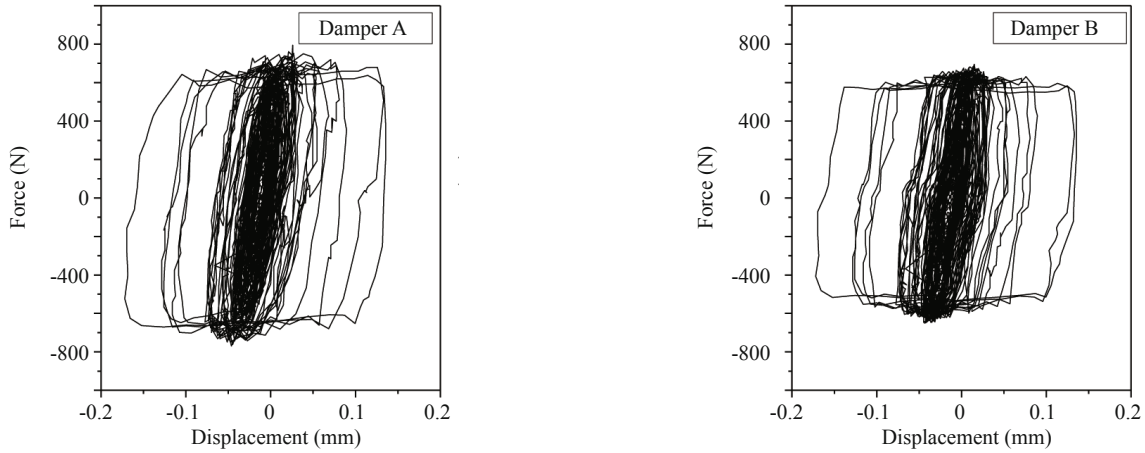

Fig. 7 Displacement-force curves for the dampers installed at story one

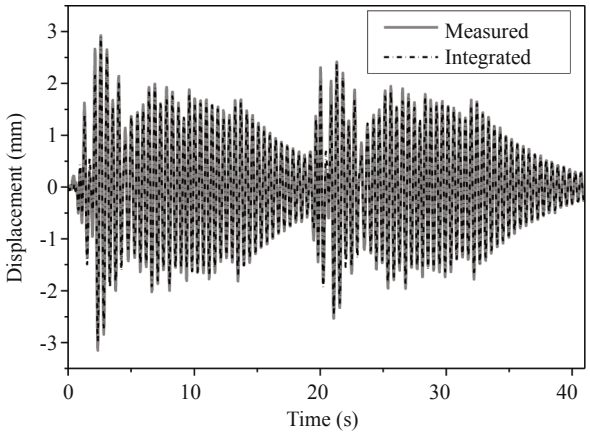

Fig. 8 Measured and integrated relative displacements at story ten from two DAQ system

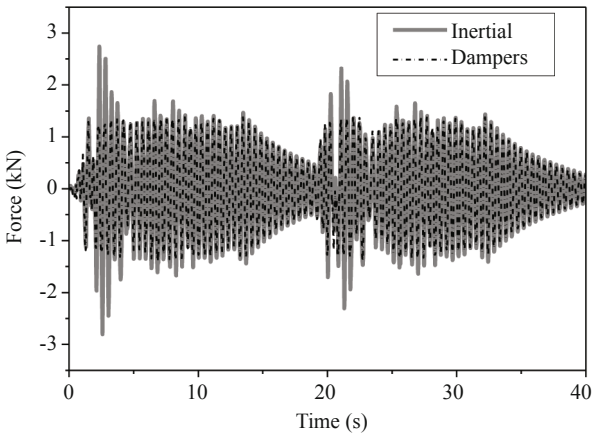

Fig. 9 Total inertial force and damper force at story one

are shown in Fig. 10. Comparing Fig. 10 with Fig. 4, it can be seen that the TFFs in Fig. 10 are totally different from those in Fig. 4, which means the MRF with added frictional dampers behaves quite different with the pure MRF and also suggests that the underlying linear system of the nonlinear system is not the same as the linear pure frame. From Fig. 10, the TFF at Story One is different from those at the other two stories, and

the difference is caused by the nonlinearity generated by the frictional dampers, which causes change in frequency magnitude and phase spectrum. To quantify the difference between the above TFFs, the log-log plots are shown in Fig. 11, where it can be seen that the TFFs also have fractal characteristics in the scale range of 2^{-4}–2^{-2}. The corresponding FDTFF are 2.455, 2.347 and 2.343 for story one, six and ten, respectively. The TFFs of the relative displacements at other stories have similar fractal characteristics, and the FDTFFs are shown in Fig. 6(b), where it can be seen that the FDTFF at story one is larger than the others. Therefore, the local nonlinearity or local damage-induced nonlinearity can be localized according to the variation of the FDTFF of the structural response.

Similarly, Fig. 12 shows the displacement-force curves for the dampers installed at story one and six. Figures 13 and 14 shows the THs, TFFs, FAS plot and log-log plot of the TFF, respectively. The FDTFFs are shown in Fig. 6(c), from which the FDTFFs at story one and six are larger than those at other stories.

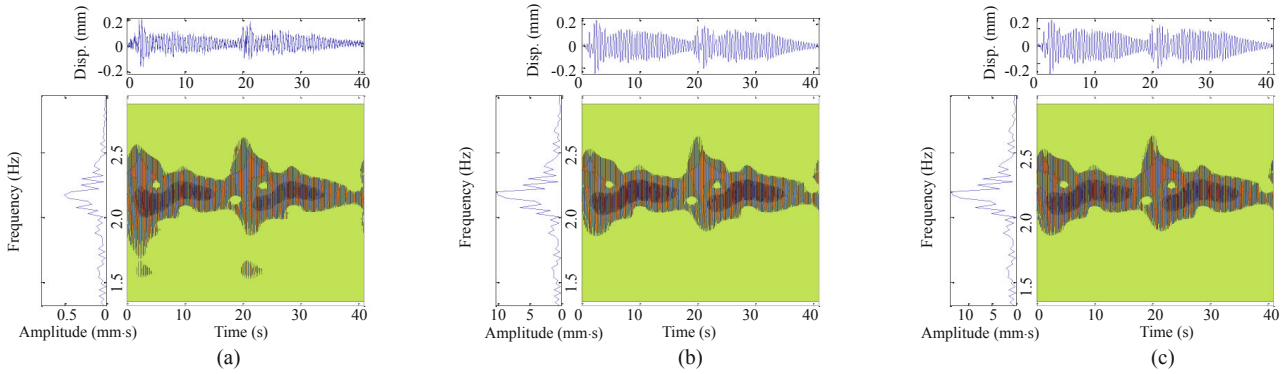

Fig. 10 The THs, TFFs and FAS of relative displacements of the MRF with frictional dampers installed at story one under El Centro ground motion: (a) story one; (b) story six; and (c) story ten

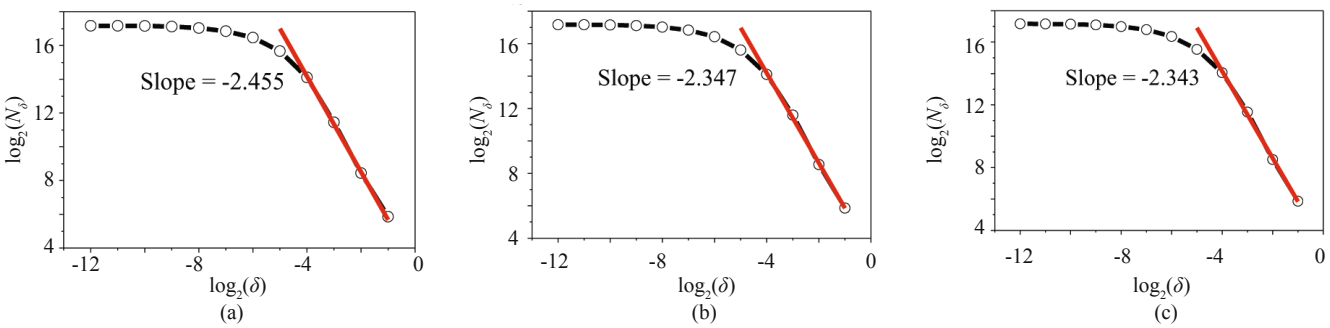

Fig. 11 Log-log plot of the box counting of the TFF of relative displacements of the MRF with frictional dampers installed at Story One under El Centro ground motion: (a) story one; (b) story six; and (c) story ten

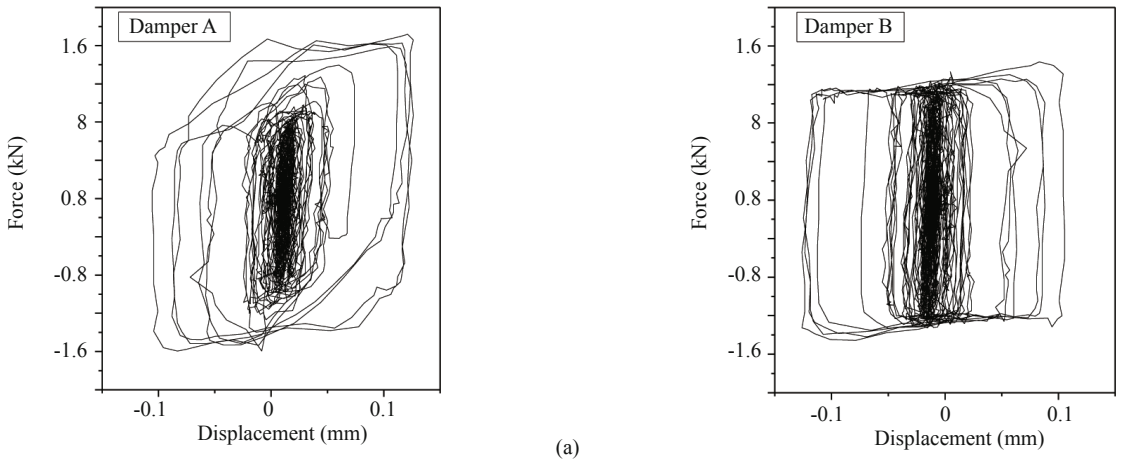

Fig. 12 Displacement-force curves for the dampers installed at story one and six: (a) story one; (b) story six

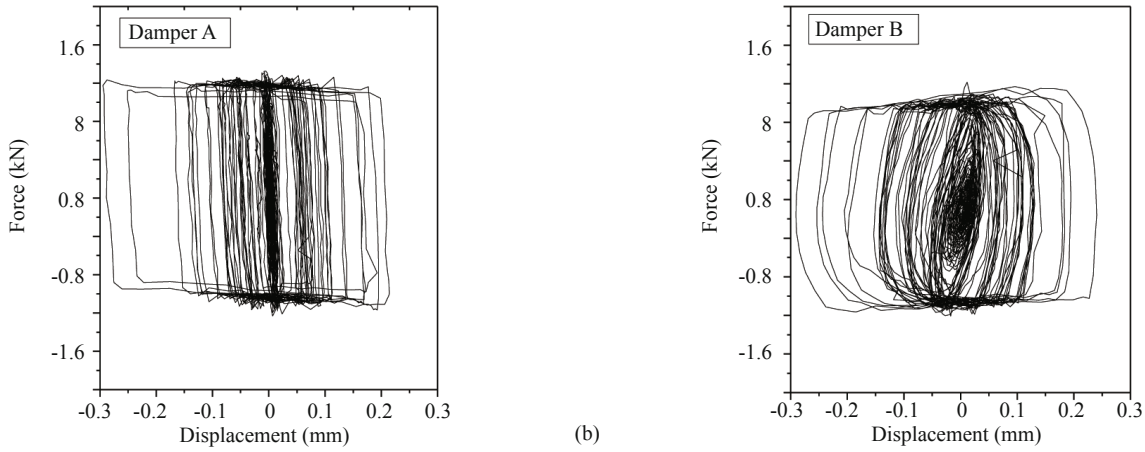

Fig . 12 Continued

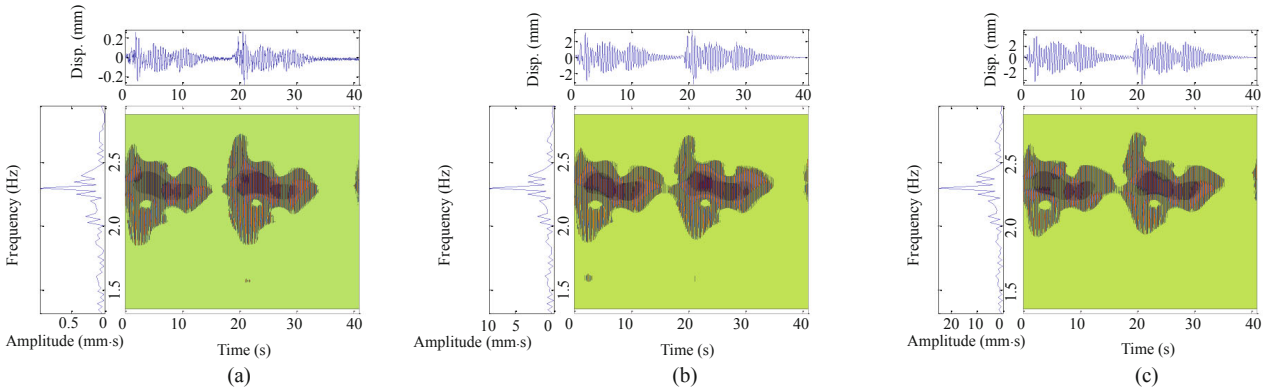

Fig. 13 The THs, TFFs and FAS of relative displacements of the MRF with frictional dampers installed at Story One and Six under El Centro ground motion: (a) story one; (b) story six; and (c) story ten

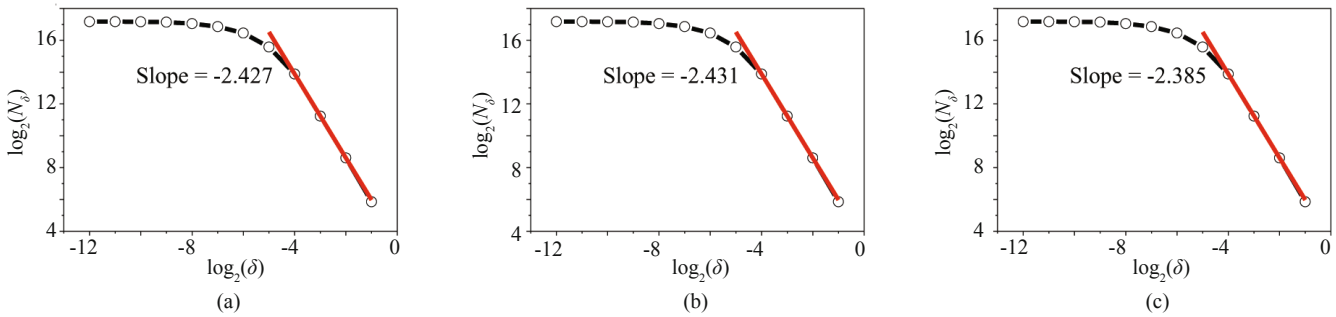

Fig. 14 Log-log plot of the box counting of the TFF of relative displacements of the MRF with frictional dampers installed at Story One and Six under El Centro ground motion: (a) story one; (b) story six; and (c) story ten

4 Conclusions

In this article, an extension of a signal-based approach formerly proposed by the authors, which compares the FDTFF of relative displacements at measured stories, is developed to detect earthquake damage of MRF, and shaking table tests have been conducted to validate the approach. The approach does not need the baseline of the health structure or the mathematical model of the structure. The test model is a 1:8 scale sixteen-story steel MRF w/o fractional dampers. The dampers are to generate single or multiple added local nonlinearities. The test results show that the approach can detect and localize added nonlinearities of MRF subjected to El Centro ground motions. Since the earthquake damage of real structure will cause the structure exhibit damage-induced nonlinear behavior such as the opening and closing of cracks in concrete and the yielding and buckling of steel, the approach can be used to detect and localize damage-induced nonlinearities of structures under strong ground motion.

Acknowledgement

This study was financially supported by the National Natural Science Foundation under Grant No. 51161120359, Ministry of Education under Grant No. 20112302110050 and Special Fund for Earthquake Scientific Research in the Public Interest under Grant No. 201308003.

Reference

Canus C, Goncalves P, Guiheneuf B and Vehel JL (2013), Available from: *http://fraclab.saclay.inria.fr/* (last accessed 26 March 2013).

Chanpheng T, Yamada H, Katsuchi H and Sasaki E (2012), "Nonlinear Features for Damage Detection on Large Civil Structures due to Earthquakes," *Structural Health Monitoring*, **11**(4): 482–488.

Doebling SW, Farrar CR, Prime MB and Shevitz DW (1996), "Damage Identification and Health Monitoring of Structural and Mechanical Systems from Changes in Their Vibration Characteristics: a Literature Review," *Report LA-13070-MS*, Los Alamos National Laboratory, Los Alamos, NM.

Farrar CR, Worden K, Todd MD, Park G, Nichols J, Adams DE, Bement MT and Farinholt K (2007), "Nonlinear System Identification for Damage Detection," *Report LA-14353S*, Los Alamos National Laboratory, Los Alamos, NM.

Hou Z, Noori M and Amand RS (2000), "Wavelet-based Approach for Structural Damage Detection," *Journal of Engineering Mechanics*, **126**(7): 677–683.

Kalkan E, Fletcher JPB, Leith WS, McCarthy J and Banga K (2012), "Real-time Seismic Monitoring of Instrumented Hospital Buildings," *USGS Fact Sheet 2012–3028*, U.S. Geological Survey, Menlo Park, CA.

Li H, Tao D, Huang Y and Bao Y (2013), "A Data-driven Approach for Seismic Damage Detection of Shear-type Building Structures Using the Fractal Dimension of Time–frequency Features," *Structural Control and Health Monitoring*, **20**(9): 1191–1210.

Loh CH, Mao CH, Chao SH and Weng JH (2010), "Feature Extraction and System Identification of Reinforced Concrete Structures Considering Degrading Hysteresis," *Structural Control and Health Monitoring*, **17**(7): 712–729.

Masri S, Sassi H and Caughey T (1982), "Nonparametric Identification of Nearly Arbitrary Nonlinear System," *Journal of Applied Mechanics*, **49**(3): 619–628.

Nagarajaiah S and Basu B (2009), "Output Only Modal Identification and Structural Damage Detection Using Time Frequency & Wavelet Techniques," *Earthquake Engineering & Engineering Vibration*, **8**(4): 583–605.

Ou J and Li H (2010), "Structural Health Monitoring in Mainland China: Review and Future Trends," *Structural Health Monitoring*, **9**(3): 219–231.

Pan TC and Lee CL (2002), "Application of Wavelet Theory to Identify Yielding in Seismic Response of Bi-linear Structures," *Earthquake Engineering and Structural Dynamics*, **31**(2): 379–398.

Park YJ, Ang AHS and Wen YK (1985), "Seismic Damage Analysis of Reinforced Concrete Buildings," *Journal of Structural Engineering*, **111**(4): 740–757.

PEER *S*trong Motion Database (2013), Available from: *http://peer.berkeley.edu/smcat/data.html* (last accessed 26 March 2013)

Qiao L and Esmaeily A (2011), "An Overview of Signal-Based Damage Detection Methods," *Applied Mechanics and Materials*, **94**: 834–851.

Rice H and Fitzpatrick J (1991), "A Procedure for the Identification of Linear and Non-linear Multi-degree-of-freedom Systems," *Journal of Sound and Vibration*, **149**(3): 397–411.

Sohn H, Farrar CR, Hemez FM, Shunk DD, Stinemates DW, Nadler BR and Czarnecki JJ (2004), "A Review of Structural Health Monitoring Literature: 1996–2001," *Report LA-13976-MS*, Los Alamos National Laboratory, Los Alamos, New Mexico.

Spanos P, Giaralis A and Politis N (2007), "Time–frequency Representation of Earthquake Accelerograms and Inelastic Structural Response Records Using the Adaptive Chirplet Decomposition and Empirical Mode Decomposition," *Soil Dynamics and Earthquake Engineering*, **27**(7): 675–689.

Todorovska MI and Trifunac MD (2007), "Earthquake Damage Detection in the Imperial County Services Building I: The Data and Time–frequency Analysis," *Soil Dynamics and Earthquake Engineering*, **27**(6): 564–576.

Wu M and Smyth AW (2007), "Application of the Unscented Kalman Filter for Real-time Nonlinear Structural System Identification," *Structural Control and Health Monitoring*, **14**(7): 971–990.